

Article

# Potential of RapidEye and WorldView-2 Satellite Data for Improving Rice Nitrogen Status Monitoring at Different Growth Stages

Shanyu Huang <sup>1,2</sup>, Yuxin Miao <sup>1,\*</sup>, Fei Yuan <sup>3</sup>, Martin L. Gnyp <sup>4</sup>, Yinkun Yao <sup>1</sup>, Qiang Cao <sup>5</sup>, Hongye Wang <sup>1</sup>, Victoria I. S. Lenz-Wiedemann <sup>1,2</sup> and Georg Bareth <sup>1,2</sup>

<sup>1</sup> International Center for Agro-Informatics and Sustainable Development (ICASD), College of Resources and Environmental Sciences, China Agricultural University, Beijing 10091, China; ivy331919@163.com (S.H.); yyk719@163.com (Y.Y.); wwwhhyy119@163.com (H.W.); victoria.lenz@uni-koeln.de (V.I.S.L.-W.); g.bareth@uni-koeln.de (G.B.)

<sup>2</sup> Institute of Geography, University of Cologne, 50923 Cologne, Germany

<sup>3</sup> Department of Geography, Minnesota State University, Mankato, MN 56001, USA; fei.yuan@mnsu.edu

<sup>4</sup> Research Centre Hanninghof, Yara International, 48249 Duellen, Germany; martin.gnyp@yara.com

<sup>5</sup> National Engineering and Technology Center for Information Agriculture, Nanjing Agricultural University, Nanjing 210095, China; qiangcao@njau.edu.cn

\* Correspondence: ymiao@cau.edu.cn or ymiao2007@gmail.com; Tel.: +86-10-6273-4676; Fax: +86-10-6273-1016

Academic Editors: Guijun Yang, Clement Atzberger and Prasad S. Thenkabail

Received: 3 January 2017; Accepted: 28 February 2017; Published: 4 March 2017

**Abstract:** For in-season site-specific nitrogen (N) management of rice to be successful, it is crucially important to diagnose rice N status efficiently across large areas within a short time frame. In recent studies, the FORMOSAT-2 satellite images with traditional blue (B), green (G), red (R), and near-infrared (NIR) wavebands have been used to estimate rice N status due to its high spatial resolution, daily revisit capability, and relatively lower cost. This study aimed to evaluate the potential improvements of RapidEye and WorldView-2 data over FORMOSAT-2 for rice N status monitoring, as the former two sensors provide additional wavelengths besides the traditional four wavebands. Ten site-year N rate experiments were conducted in Jiansanjiang, Heilongjiang Province of Northeast China from 2008 to 2011. Plant samples and field hyperspectral data were collected at three growth stages: panicle initiation (PI), stem elongation (SE), and heading (HE). The canopy-scale hyperspectral data were upscaled to simulate the satellite bands. Vegetation index (VI) analysis, stepwise multiple linear regression (SMLR), and partial least squares regression (PLSR) were performed to derive plant N status indicators. The results indicated that the best-performed VIs calculated from the simulated RapidEye and WorldView-2 bands, especially those based on the red edge (RE) bands, explained significantly more variability for above ground biomass (AGB), plant N uptake (PNU), and nitrogen nutrition index (NNI) estimations than their FORMOSAT-2-based counterparts did, especially at the PI and SE stages. The SMLR and PLSR models based on the WorldView-2 bands generally had the best performance, followed by the ones based on the RapidEye bands. The SMLR results revealed that both the NIR and RE bands were important for N status estimation. In particular, the NIR1 band (760–900 nm from RapidEye or 770–895 nm from WorldView-2) was most important for estimating all the N status indicators. The RE band (690–730 nm or 705–745 nm) improved AGB, PNU, and NNI estimations at all three stages, especially at the PI and SE stages. AGB and PNU were best estimated using data across the stages while plant N concentration (PNC) and NNI were best estimated at the HE stage. The PLSR analysis confirmed the significance of the NIR1 band for AGB, PNU, and NNI estimations at all stages except for the HE stage. It also showed the importance of including extra bands (coastal, yellow, and NIR2) from the WorldView-2 sensor for N status estimation. Overall, both the RapidEye and WorldView-2 data with RE bands improved the results relative to FORMOSAT-2 data. However, the WorldView-2 data with three extra bands in the visible and NIR regions showed the highest potential in estimating rice N status.

**Keywords:** FORMOSAT-2; satellite remote sensing; nitrogen nutrition index; red edge; precision nitrogen management

---

## 1. Introduction

Precision nitrogen (N) management of rice (*Oryza sativa* L.) is crucially important for food security and sustainable development, especially for Asian countries like China [1–3]. Non-destructive technologies are needed for in-season site-specific diagnosis of rice plant N status and making topdressing N recommendations. During the past decade, active canopy sensors (ACS), such as GreenSeeker (Trimble Navigation Limited, Sunnyvale, CA, USA) and Crop Circle (Holland Scientific, Lincoln, NE, USA) sensors, have been developed and have gained popularity for diagnosing crop N status and guiding in-season N management of wheat (*Triticum aestivum* L.), maize (*Zea mays* L.), and rice [1,4–8]. For large production field applications, such sensors have been installed on variable rate fertilizer application machines for real-time sensing, diagnosis of crop N status, topdressing or side-dressing N recommendation, and variable rate application [9–11]. However, such systems are not common for rice, as it is difficult for variable rate application machines to enter flooded paddy fields. It is also very challenging and time-consuming to carry active canopy sensors and walk across large paddy fields.

Alternatively, satellite remote sensing offers a promising non-intrusive solution to monitor rice N status and to guide site-specific N recommendations over large areas [3,12,13]. For in-season site-specific N management, a satellite sensor with relatively high spatial resolution is required because rice canopy plots are small. In addition, high temporal resolution is also crucially important, as cloudy weather conditions are quite common in rice planting regions. There is only a narrow time window to collect and process remote sensing images, produce topdressing fertilization prescription, and implement fertilizer applications. Therefore, to date, studies of using satellite instruments for crop N monitoring are still limited due to the restricted sensor resolutions of most satellites.

The FORMOSAT-2 is the first earth observation satellite developed by the National Space Organization (NSPO) of Taiwan in 2004. The FORMOSAT-2 data have a spatial resolution of 8 m for the four multispectral bands (Blue (B), Green (G), Red (R), and Near Infrared (NIR)) and 2 m for the panchromatic band. The daily revisit capability with a constant view angle and the medium-high spatial resolution make FORMOSAT-2 one of the most suitable satellites for regional precision agriculture applications [3,14]. Particularly, Huang et al. (2015) [3] found that FORMOSAT-2 images could be used to estimate rice aboveground biomass (AGB), leaf area index (LAI), plant N uptake (PNU) and N nutrition index (NNI) at early growth stage. In addition, the IKONOS and QuickBird satellite sensors have higher spatial resolutions but lower temporal resolutions than FORMOSAT-2 with the same band settings. They also have been used in previous studies for monitoring crop N status, green LAI (GLAI), and yield [15–17].

Launched in August of 2008, RapidEye was the first commercial satellite with a red edge (RE) band in addition to traditional B, G, R, and NIR bands, with an improved 5 m spatial resolution [18]. Many studies evaluated the applicability of the RE waveband. Eitel et al. (2007) [19] used hyperspectral data to simulate RapidEye wavebands and found that the RE-based vegetation index (VI), Modified Chlorophyll Absorption Ratio Index/Modified Triangular Vegetation Index 2 (MCARI/MTVI2), performed the best for chlorophyll content and leaf N concentration estimations. Eitel et al. (2011) [20] stated that the RE-based VI, Normalized Difference Red Edge (NDRE), could identify plant N stress earlier than Normalized Difference Vegetation Index (NDVI) and Green NDVI (GNDVI). The RE-based indices from the RapidEye images improved the LAI and plant N status estimations compared with the R radiation-based VIs [21–23].

In addition to RapidEye, the WorldView-2 satellite was launched in October of 2009 with a further increased spatial resolution of 2 m. Besides the traditional four and the RE wavebands, three additional

ones are included: coastal (C), yellow (Y), and an extra NIR band (NIR2). Mutanga et al. (2012) [24] found that the NDRE using WorldView-2 imagery could solve the saturation problem encountered with high-density biomass estimation for wetland vegetation.

The FORMOSAT-2, RapidEye, and WorldView-2 satellites are ideal choices for crop N status estimation since they all have short revisit time with 2–8 m spatial resolutions. Notably, both the RapidEye and WorldView-2 satellite sensors with additional wavelengths have the potential to further improve crop N monitoring. The first crucial question addresses how to define the expected improvements of RapidEye data for rice N status monitoring compared with FORMOSAT-2 data. Second, can WorldView-2 data further improve the estimation of rice N status with three extra spectral bands compared with RapidEye? Comparing these three satellite datasets directly proves difficult because of the lacking of archived images from these satellite sensors at multiple growth stages for this study site on our sampling dates. To evaluate and quantify the potential benefits of the RE band or the additional three bands, a practical approach is to use hyperspectral canopy reflectance data to simulate the spectral bands of the three satellite sensors. This approach has been widely used in remote sensing studies in recent years. Yang et al. (2008) [25] found that the NDVI values calculated with a hyperspectral canopy sensor were highly correlated ( $R^2 = 0.79$ ) with NDVIs derived from broadband FORMOSAT-2 images. Bsaibes et al. (2008) [26] compared the ground measured albedo and FORMOSAT-2 retrievals for five crops and found their albedo values were closely related. Bausch et al. (2010) [27] compared several normalized VIs based on QuickBird imagery with the ones calculated from simulated QuickBird bands using hyperspectral data, and confirmed their high levels of similarity.

In previous studies, VIs have been widely used to estimate crop N status. While numerous VIs have been developed, the most commonly used VIs are based on R and NIR bands, such as the NDVI. However, the NDVI may saturate under moderate-to-high biomass conditions at later growth stages [28–30]. The RE-based VIs have been proven to be sensitive to crop canopy chlorophyll and N variation, even under the high biomass condition [7,31–34]. Since both RapidEye and WorldView-2 have the RE band, the question of how RE-based indices could improve the estimation of rice N status needed to be answered. In addition to VI analysis, the stepwise multiple linear regression (SMLR) and partial least squares regression (PLSR) were applied as well since it was noted that multivariate techniques have usually allowed slightly better N prediction than the VI method [35]. The PLSR analysis combines the methods of principal component analysis (PCA) and multiple linear regression that cut the predictors to a smaller and uncorrelated subset. Therefore, it can efficiently deal with the multi-collinearity issue in predicting variables [36]. PLSR has been used successfully to estimate canopy biomass and N status in wheat crops [37] and to assess rice leaf growth and N status [38].

Therefore, the objective of this study was to evaluate the potential of using RapidEye and WorldView-2 satellite data to improve rice N status monitoring over commonly used four-band satellite data such as FORMOSAT-2 at different growth stages based on ground hyperspectral canopy data and VI analysis, SMLR as well as PLSR.

## 2. Materials and Methods

### 2.1. Study Area

The study area is located at the Qixing Farm in the Sanjiang Plain, Heilongjiang Province, Northeast China. The Sanjiang Plain used to be a wild natural wetland formed by the alluvium of three river systems—Heilong River, Songhua River, and Wusuli River. This area has a typical cool-temperate sub-humid continental monsoon climate. During the growing season (April–October), the average rainfall is around 400 mm, which accounts for approximately 70% of yearly precipitation. The mean annual temperature is about 2 °C [39], and the average daily temperature is 19.9 °C during the growing season (from mid-May to mid-September). The annual sunshine duration is 2300–2600 h, and the whole year frost-free period is about 120–140 days [40]. The main soil type in the region

is Albic soil, classified as Mollic Planosols in the FAO-UNESCO system and Typical Argialbolls in Soil Taxonomy [41].

Two sites were selected to conduct 10 N rate experiments. Site 1 (47°15'52"N, 132°39'05"E) has been planted with rice since 1992 and at Site 2 (47°13'59"N, 132°38'50"E) rice planting started in 2002.

## 2.2. Experimental Design

Ten N rate experiments were conducted in 2008, 2009, and 2011, involving two Japonica rice cultivars: Kongyu 131 (11 leaves) and Longjing 21 (12 leaves) (Table 1). All of the experiments adopted the randomized complete block design with 3–4 replications. The N fertilizer was applied in three splits for Experiments 1–6: 40%–45% as the basal application before transplanting, 20%–30% at the tillering stage, and 30%–35% at the stem elongation (SE) stage. For Experiments 7–10, the N fertilizer was applied in two splits: 60% as the basal application and 40% at the tillering stage. In each experiment, 45–60 kg·ha<sup>-1</sup> phosphate (P<sub>2</sub>O<sub>5</sub>) and 90–105 kg·ha<sup>-1</sup> potash (K<sub>2</sub>O) fertilizers were applied to ensure sufficient phosphorus (P) and potassium (K) nutrients. The P fertilizer was applied as a basal application before transplanting while the K fertilizer was applied in two splits, with 50% as the basal fertilizer and 50% as the panicle fertilizer at the SE stage.

**Table 1.** Details of the nitrogen rate experiments conducted from 2008 to 2011 in Jiansanjiang, Heilongjiang Province, Northeast China.

Experiment	Site	Year	Cultivar	N Rates (kg·ha <sup>-1</sup> )	Transplanting/Harvesting Date	Sampling Stage
1	1	2008	Kongyu 131	0, 35, 70, 105, 140	29 May/21 September	PI, SE, HE
2	2	2008	Kongyu 131	0, 35, 70, 105, 140	13 May/22 September	PI, SE, HE
3	1	2009	Kongyu 131	0, 35, 70, 105, 140	24 May/27 September	SE, HE
4	2	2009	Kongyu 131	0, 35, 70, 105, 140	20 May/27 September	PI, SE, HE
5	1	2011	Kongyu 131	0, 70, 100, 130, 160	17 May/21 September	PI
6	1	2011	Longjing 21	0, 70, 100, 130, 160	19 May/21 September	PI
7	1	2008	Kongyu 131	0, 23, 45, 68, 91	29 May/21 September	HE
8	2	2008	Kongyu 131	0, 23, 45, 68, 91	13 May/22 September	HE
9	1	2009	Kongyu 131	0, 23, 45, 68, 91	24 May/27 September	SE, HE
10	2	2009	Kongyu 131	0, 23, 45, 68, 91	20 May/27 September	SE, HE

PI: panicle initiation stage; SE: stem elongation stage; HE: heading stage.

## 2.3. Determining N Status Indicators with Plant Sampling and Analysis

Plant samples were collected at several critical growth stages, including the panicle initiation (PI), SE and heading (HE) stages, to determine the values of four N status indicators—AGB, plant N concentration (PNC), PNU, and NNI. Growth stages have significant impacts on estimating N status indicators. The AGB and PNU increase with the advancement of growth stages, and they have positive correlations with N nutritional status. As explained by the dilution effect [42,43], the PNC declines during the growth period within dense canopies. It is positively correlated with N nutritional status but inversely related with growth stages.

The detailed sampling dates and related information were listed in Table 1. Before plant sampling, the average tiller number per hill for each treatment plot was determined, and then 3 to 6 representative hills with average tiller numbers were randomly selected and cut at ground surface. All the plant samples were rinsed with water and the roots were removed to determine the AGB. Then the samples were separated into leaves, stems, and panicles (for samples collected at the HE stage). The separated samples were put into an oven at 105 °C for half an hour for deactivation of enzymes, and then dried at 70–80 °C until constant weight. After being weighed, the samples were ground into powders and sub-samples were put through 1 mm sieve for PNC analysis using the standard Kjeldahl-N method. The PNU was determined by multiplying PNC with dry AGB. Both PNC and PNU have been widely used as N status indicators in former studies.

NNI is defined as the ratio of the actual PNC (N<sub>a</sub>) and the critical N concentration (N<sub>c</sub>), which was calculated using the equation developed for rice in Northeast China based on data from N rate experiments conducted in this region from 2008 to 2013 following the method of Justes et al. (1994) [44].

More details about the method can be found in Huang et al. (2015) [3]. NNI is a unitless parameter. It increases with increasing N rates. This trend remains constant during the growth period [45,46]. If  $N_a$  is greater than  $N_c$  ( $NNI > 1$ ), it indicates a surplus of N while the opposite is true if  $N_a$  is smaller than  $N_c$  ( $NNI < 1$ ). An NNI value of 1 indicates an optimal N supply [3,43]. NNI has advantages as a specific, sensitive, memorable, and predictive tool for crop N diagnosis [43,47]. Therefore, NNI is a better indicator for diagnosing crop N status than PNC and PNU [43]. The NNI map can be used directly to guide in-season topdressing N applications [3,48].

#### 2.4. Field Spectral Measurements and Re-Sampling

The rice canopy spectra were collected using portable hyperspectral instruments FieldSpec3 (Analytical Spectral Devices Inc., Boulder, CO, USA) for Experiments 1–4 and 7–10, and QualitySpec Pro (Analytical Spectral Devices Inc., Boulder, CO, USA) for Experiments 5 and 6. The QualitySpec Pro collects reflectance from 350 to 1800 nm while the FieldSpec 3 provides spectra across 350 to 2500 nm. Both of them have a spectral resolution of 1.2 nm from 350 to 1100 nm and a 2 nm spectral resolution beyond 1100 nm.

All spectra were obtained under sunny cloudless conditions during local mid-day (9:00 a.m.–1:00 p.m.). The measurements were taken 0.3 m above the canopy with a 25° field of view, which gave a sample diameter of 0.14 m. The sensors were carried along the north side of the rice plant rows to minimize the disturbance of the canopy structure and avoid the creation of shadows. The reflectance values were calibrated by a barium sulfate ( $BaSO_4$ ) reference panel at least every 10–15 min. Five to six scans were taken randomly for each plot. The average value was calculated subsequently and used as the plot reflectance.

Next, the FORMOSAT-2 (F2), RapidEye (RY), and WorldView-2 (WV2) bands were simulated and evaluated. Detailed sensor characteristics for the three satellite systems were shown in Table 2. The field hyperspectral data were resampled in order to simulate the satellite wavebands based on the theory of band equivalent reflectance explained as Equation (1):

$$r_i = \frac{\sum_{\lambda u_i}^{\lambda l_i} r(\lambda) \varphi_i(\lambda)}{\sum_{\lambda u_i}^{\lambda l_i} \varphi_i(\lambda)} \quad (1)$$

where  $r_i$  stands for the reflectance of band  $i$ ;  $\lambda u_i$  is the starting wavelength of band  $i$ ;  $\lambda l_i$  is the termination wavelength of band  $i$ ;  $r(\lambda)$  is the reflectance value at wavelength  $\lambda$ ;  $\varphi_i(\lambda)$  is the band response function of band  $i$  at wavelength  $\lambda$ . The band response function data of FORMOSAT-2 were provided by the NSPO while the corresponding data for RapidEye and WorldView-2 were supplied by the ENVI 4.8 software (Harris Geospatial Solutions, Broomfield, CO, USA) (Figure 1).

**Table 2.** The properties of the FORMOSAT-2, RapidEye, and WorldView-2 satellite sensors.

Properties	FORMOSAT-2 (F2)	RapidEye (RY)	WorldView-2 (WV2)
Type	Sun-synchronous	Sun-synchronous	Sun-synchronous
Launch time	4 May 2004	8 August 2008	9 October 2009
Orbit altitude (km)	891	620	770
Spatial Resolution for Multispectral bands (m)	8	6.5	2
Spatial Resolution for Panchromatic bands (m)	2	-	0.5
Revisit time (Day)	1	<1	1.1
Swath width (km)	24	80	16.4
Band settings	450–520 nm (Blue: FB) 520–600 nm (Green: FG) 630–690 nm (Red: FR) 760–900 nm (NIR1: FNIR1)	440–510 nm (Blue: RB) 520–590 nm (Green: RG) 630–685 nm (Red: RR) 690–730 nm (Red edge: RRE) 760–900 nm (NIR1: RNIR1)	400–450 nm (Coastal: WVC) 450–510 nm (Blue: WVB) 510–581 nm (Green: WVG) 585–625 nm (Yellow: WVY) 630–690 nm (Red: WVR) 705–745 nm (Red Edge: WVRE) 770–895 nm (NIR1: WVNIR1) 860–1040 nm (NIR2: WVNIR2)

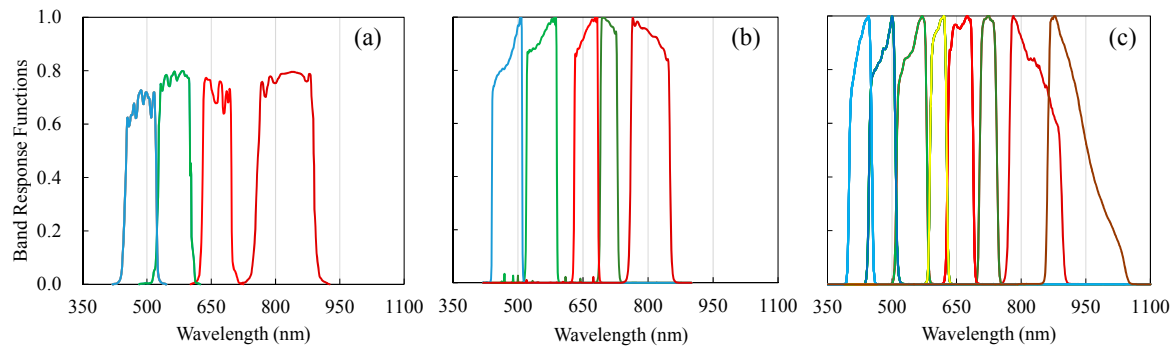


**Figure 1.** Band response functions for: FORMOSAT-2 (a); RapidEye (b); and WorldView-2 (c) satellite sensors used in this study.

## 2.5. Data Analysis

All 369 in-situ samples were divided into two groups by a stratified random sampling method, with approximately 2/3 of the data used for model calibration and the rest for model validation.

In total, 21 different VIs were calculated (Table 3) and correlated with the four N status indicators separately. To evaluate the band effects of simulated satellite data on the relationships between VIs and N status indicators over the growing season, the same VIs were calculated for all three types of satellite data when possible. Linear regression models were then constructed for the three individual growth stages and across the stages. The relationships between each of the VIs and each of the indicators were determined. The coefficient of determination ( $r^2$ ) was used to assess and compare the performance of the VI models. According to the  $r^2$  ranking, the top 5 VIs were listed, and the best VIs were shown in scatter plots. The Root Mean Square Error (RMSE) and relative error (REr) were also calculated to evaluate the model performance.

**Table 3.** Vegetation indices evaluated in this study for estimating rice N status indicators.

Vegetation Index	Formula	Satellite Sensors	Reference
Ration Vegetation Index (RVI)	NIR/R	F2, RY, WV2	[49]
Chlorophyll Index (CI)	(NIR/G) – 1	F2, RY, WV2	[50]
Normalized Difference Vegetation Index (NDVI)	(NIR – R)/(NIR + R)	F2, RY, WV2	[51]
Green NDVI (GNDVI)	(NIR – G)/(NIR + G)	F2, RY, WV2	[52]
Optimized Soil Adjusted Vegetation Index (OSAVI)	$(1 + 0.16) \times ((\text{NIR} - \text{R}) / (\text{NIR} + \text{R} + 0.16))$	F2, RY, WV2	[53]
Modified Chlorophyll Absorption in Reflectance Index (MCARI)	$((\text{NIR} - \text{R}) - 0.2(\text{R} - \text{G})) \times (\text{NIR} / \text{R})$	F2, RY, WV2	[54]
Triangular Vegetation Index (TVI)	$0.5 \times (120(\text{NIR} - \text{G}) - 200(\text{R} - \text{G}))$	F2, RY, WV2	[55]
Modified Transformed Chlorophyll Absorption in Reflectance Index (TCARI)	$3 \times ((\text{NIR} - \text{R}) - 0.2(\text{NIR} - \text{G})(\text{NIR} / \text{R}))$	F2, RY, WV2	[56]
MCARI/OSAVI	MCARI/OSAVI	F2, RY, WV2	[56]
TCARI/OSAVI	TCARI/OSAVI	F2, RY, WV2	[56]
Red Edge Chlorophyll Index (RECI)	(NIR/RE) – 1	RY, WV2	[50]
Normalized difference Red Edge Index (NDRE)	(NIR – RE)/(NIR + RE)	RY, WV2	[57]
MERIS Terrestrial Chlorophyll Index (MTCI)	(NIR – RE)/(RE – R)	RY, WV2	[58]
Canopy Chlorophyll Content Index (CCCI)	$(\text{NDRE} - \text{NDRE}_{\text{min}}) / (\text{NDRE}_{\text{max}} - \text{NDRE}_{\text{min}})$	RY, WV2	[57]
Nitrogen Planar Domain Index (NDPI)	$(\text{RECI} - \text{RECI}_{\text{min}}) / (\text{RECI}_{\text{max}} - \text{RECI}_{\text{min}})$	RY, WV2	[59]
Red Edge OSAVI (REOSAVI)	$(1 + 0.16) \times ((\text{NIR} - \text{RE}) / (\text{NIR} + \text{RE} + 0.16))$	RY, WV2	[60]
Red Edge MCARI (REMCARI)	$((\text{NIR} - \text{RE}) - 0.2(\text{RE} - \text{G})) \times (\text{NIR} / \text{RE})$	RY, WV2	[60]
Red Edge Triangular Vegetation Index (RETVI)	$0.5 \times (120(\text{NIR} - \text{G}) - 200(\text{RE} - \text{G}))$	RY, WV2	[55]
Red Edge TCARI (RETCARI)	$3 \times ((\text{NIR} - \text{RE}) - 0.2(\text{NIR} - \text{G})(\text{NIR} / \text{RE}))$	RY, WV2	[60]
REMCARI/REOSAVI	REMCARI/REOSAVI	RY, WV2	[60]
RETCARI/REOSAVI	RETCARI/REOSAVI	RY, WV2	[60]

In addition, SMLR using SPSS V.20.0 (IBM SPSS Statistics, Armonk, NY, USA) and PLSR using Matlab 7.10 (MathWorks, Natick, MA, USA) were implemented to estimate the four variables. In order to evaluate the relative importance of each waveband in each of the PLSR models, the Variable Importance in Projection (VIP) values were computed. The VIP is a variable selection method in PLSR. It calculates the influence of the independent variables to the dependent variable, and selects the most influential predictors for a PLSR model. The VIP value for a variable is a weighted sum of squares of the PLSR weights that takes into account the explained variance of each PLSR dimension. A variable with a VIP value greater than one is considered important in the PLSR model. The larger the VIP score, the greater the contribution of the variable. The VIP values can be used to identify individual waveband importance and the most effective spectral regions [61,62].

### 3. Results

#### 3.1. Variability of the N Status Indicators

The descriptive statistics of the four N status indicators at different growth stages for both of the calibration and validation datasets were listed in Table 4. In the calibration dataset, both AGB and PNU increased moderately from the PI stage to the SE stage, and dramatically to the HE stage. In contrast, PNC decreased slightly from the PI stage to the SE stage, and declined sharply to the HE stage, affected by the “dilution effect” described by Plénet and Lemaire (1999) [61]. The NNI indicated a slightly under-supply of N at the PI stage, but a nearly optimal N supply at the SE stage and an over-supply at the HE stage. The AGB and PNU had larger coefficients of variation (CVs) than PNC and NNI (Table 4). Similar trends were observed for the validation dataset. The mean values of the four N indicators across stages were similar for both datasets.

**Table 4.** Descriptive statistics of the measured aboveground biomass (AGB), nitrogen concentration (PNC), plant N uptake (PNU), and nitrogen nutrition index (NNI) for the model estimation and validation at the panicle initiation (PI), stem elongation (SE), heading (HE) and across stages (All).

Stage	Calibration Dataset				Validation Dataset				
		AGB (t·ha <sup>-1</sup> )	PNC (%)	PNU (kg·ha <sup>-1</sup> )	NNI	AGB (t·ha <sup>-1</sup> )	PNC (%)	PNU (kg·ha <sup>-1</sup> )	NNI
PI	N	57	57	57	57	28	28	28	28
	Mean	1.11	2.47	27.53	0.96	1.05	2.46	26.09	0.94
	SD	0.50	0.17	12.71	0.11	0.48	0.21	11.84	0.10
	CV	45.02	6.97	46.17	11.4	45.79	8.45	45.40	10.63
SE	N	92	92	92	92	45	45	45	45
	Mean	1.78	2.36	40.13	1.01	1.83	2.39	41.32	1.02
	SD	0.88	0.36	16.96	0.14	0.99	0.35	18.25	0.12
	CV	49.36	15.11	42.26	13.74	54.17	14.64	44.17	12.04
HE	N	98	98	98	98	49	49	49	49
	Mean	6.28	1.62	103.34	1.09	5.93	1.6	95.41	1.05
	SD	1.49	0.28	36.2	0.24	1.45	0.29	31.09	0.22
	CV	23.75	17.06	35.03	21.97	24.46	18.11	32.59	21.18
All	N	247	247	247	247	122	122	122	122
	Min	0.20	0.83	4.39	0.53	0.14	0.96	3.17	0.65
	Max	9.92	3.15	205.64	1.63	9.21	3.35	195.37	1.63
	Mean	3.41	2.09	62.30	1.03	3.30	2.09	59.55	1.02
	SD	2.59	0.48	42.36	0.19	2.45	0.50	37.94	0.17
	CV	75.95	22.97	67.99	18.45	74.24	23.92	63.71	16.67

N: number of observations; SD: standard deviation; CV: coefficient of variation (%).

#### 3.2. Correlation between N Indicators and Vegetation Indices

For VI models derived from RapidEye and WorldView-2 bands, all the top five ones for AGB (Table 5) and PNU (Table 6) estimations were based on RE indices—MERIS Terrestrial Chlorophyll Index (MTCI), Canopy Chlorophyll Content Index (CCCI), N Planar Domain Index (NDPI), Red Edge Chlorophyll Index (RECI), and NDRE. Comparatively, the top five FORMOSAT-2-based VI models showed significantly lower performance at the PI and SE stages and slightly lower performance at the HE stage and across the stages, demonstrating the importance of using RE band in AGB and PNU

estimations at early and middle growth stages. From the PI through the HE stages, the best performed RE VI models showed  $r^2$  values ranging from 0.62 to 0.65 for PNU estimation (Table 6). Across the stages, the RE-based NDPI, RECI, MTCI and the traditional Chlorophyll Index (CI) explained the most variability for AGB and PNU estimations with  $r^2$  ranging from 0.80 to 0.83 (Figure 2).

In contrast, as shown in Table 5, PNC did not have any significant relationships with most of the VIs at the PI and SE stages, indicating the difficulty of estimating N concentrations at early and middle stages using VIs. However, at the HE stage, the model performance was significantly improved with the highest  $r^2$  ranging from 0.42 to 0.57. Again, the RE-based indices performed better at this stage. Across the stages, similar performance was obtained for both groups of indices. In addition, Table 6 revealed an improved NNI estimation using RE-based VIs relative to the non-RE ones. The performance gap between the two groups of indices was the smallest at the SE stage. Likewise, the best RE-based VI models ( $r^2 = 0.60\text{--}0.62$ ) for NNI estimation were found to be at the HE stage, slightly better than the original CI ( $r^2 = 0.58$ ) and GNDVI ( $r^2 = 0.57$ ) models. These results demonstrated that the best stage for PNC and NNI estimations based on these satellite sensor bands was the HE stage. For FORMOSAT-2-based indices, the CI was the best for estimating these N indicators in most cases (Figure 2).

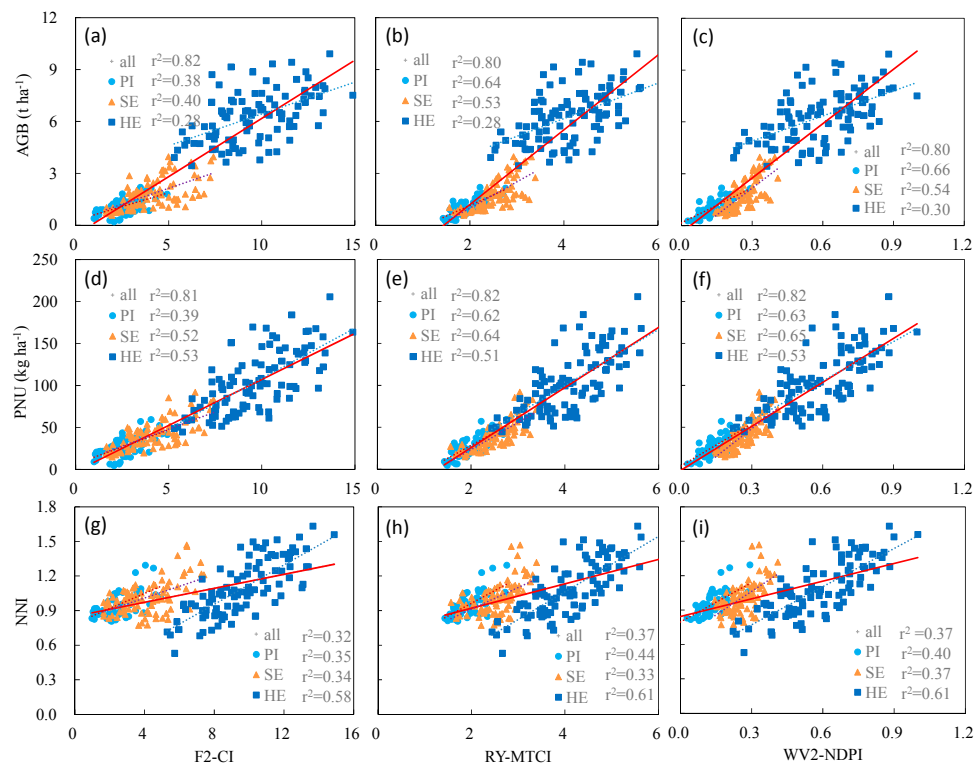


**Figure 2.** Relationships between: FORMOSAT-2-based Chlorophyll Index (CI) (a); RapidEye-based MERIS Terrestrial Chlorophyll Index (MTCI) (b); WorldView-2-based Nitrogen Planar Domain Index (NDPI) (c), and aboveground biomass (AGB); FORMOSAT-2-based CI (d); RapidEye-based MTCI (e); WorldView-2-based NDPI (f), and plant N uptake (PNU); and FORMOSAT-2-based CI (g); RapidEye-based MTCI (h); WorldView-2-based NDPI (i), and N nutrition index (NNI), at the panicle initiation (PI), stem elongation (SE), heading (HE), and across all stages. The relationships between VIs and N status indicators across growth stages are indicated by the red lines.

**Table 5.** The top five coefficients of determination ( $r^2$ ) for the relationships between vegetation indices based on the wavebands of FORMOSAT-2 (F2), RapidEye (RY), WorldView-2 (WV2) and aboveground biomass (AGB), plant N concentration (PNC) at the panicle initiation (PI), stem elongation (SE), heading (HE), and across stages (All), respectively. Only significant  $r^2$  values were listed.

PI Stage		SE Stage		HE Stage		All	
Index	AGB	Index	AGB	Index	AGB	Index	AGB
F2-CI	0.39 **	F2-GNDVI	0.41 **	F2-CI	0.28 **	F2-CI	0.82 **
F2-GNDVI	0.35 **	F2-OSAVI	0.41 **	F2-GNDVI	0.27 **	F2-RVI	0.80 **
F2-MCARI/OSAVI	0.33 **	F2-NDVI	0.41 **	F2-RVI	0.21 **	F2-MCARI/OSAVI	0.77 **
F2-TCARI/OSAVI	0.34 **	F2-CI	0.40 **	F2-NDVI	0.20 **	F2-TCARI/OSAVI	0.77 **
F2-RVI	0.33 **	F2-TVI	0.39 **	F2-TCARI/OSAVI	0.18 **	F2-MCARI	0.75 **
RY-MTCI	0.64 **	RY-MTCI	0.53 **	RY-MTCI	0.28 **	RY-CI	0.82 **
RY-CCCI	0.61 **	RY-CCCI	0.51 **	RY-CCCI	0.28 **	RY-RECI	0.81 **
RY-NDPI	0.59 **	RY-NDPI	0.50 **	RY-NDPI	0.28 **	RY-NDPI	0.81 **
RY-RECI	0.46 **	RY-RECI	0.47 **	RY-RECI	0.28 **	RY-RVI	0.80 **
RY-NDRE	0.43 **	RY-NDRE	0.46 **	RY-NDRE	0.28 **	RY-MTCI	0.80 **
WV2-NDPI	0.65 **	WV2-MTCI	0.57 **	WV2-NDPI	0.30 **	WV2-CI	0.82 **
WV2-MTCI	0.62 **	WV2-NDPI	0.54 **	WV2-MTCI	0.30 **	WV2-RECI	0.82 **
WV2-RETVI	0.57 **	WV2-RECI	0.51 **	WV2-RECI	0.30 **	WV2-MTCI	0.81 **
WV2-RECI	0.54 **	WV2-NDRE	0.50 **	WV2-NDRE	0.30 **	WV2-RETVI	0.81 **
WV2-NDRE	0.53 **	WV2-RETVI	0.47 **	WV2-CCCI	0.30 **	WV2-NDPI	0.80 **
Index	PNC	Index	PNC	Index	PNC	Index	PNC
F2-CI		F2-NDVI	0.06 *	F2-CI	0.53 **	F2-OSAVI	0.42 **
F2-GNDVI		F2-GNDVI		F2-GNDVI	0.52 **	F2-TVI	0.41 **
F2-RVI		F2-OSAVI		F2-NDVI	0.46 **	F2-NDVI	0.39 **
F2-TCARI/OSAVI		F2-CI		F2-RVI	0.44 **	F2-RVI	0.39 **
F2-TCARI		F2-RVI		F2-TCARI/OSAVI	0.42 **	F2-GNDVI	0.39 **
RY-RETCARI/REOSAVI		RY-RETCARI	0.09 **	RY-RECI	0.57 **	RY-OSAVI	0.42 **
RY-GNDVI		RY-NDVI	0.06 *	RY-MTCI	0.56 **	RY-REOSAVI	0.42 **
RY-RECI		RY-NDRE	0.05 *	RY-NDPI	0.56 **	RY-TVI	0.41 **
RY-NDPI		RY-MTCI		RY-NDRE	0.55 **	RY-GNDVI	0.40 **
RY-MTCI		RY-GNDVI		RY-RETCARI/REOSAVI	0.55 **	RY-RETVI	0.40 **
WV2-GNDVI		WV2-MTCI	0.07 *	WV2-REOSAVI	0.57 **	WV2-RETCARI	0.44 **
WV2-RECI		WV2-NDVI	0.06 *	WV2-RECI	0.56 **	WV2-OSAVI	0.42 **
WV2-NDPI		WV2-NDRE	0.05 *	WV2-MTCI	0.56 **	WV2-REOSAVI	0.41 **
WV2-NDRE		WV2-GNDVI		WV2-NDRE	0.56 **	WV2-TVI	0.41 **
WV2-CI		WV2-RECI		WV2-NDPI	0.55 **	WV2-GNDVI	0.39 **

\*\* Correlation is significant at the  $p < 0.01$  level; \* Correlation is significant at the  $p < 0.05$  level.

**Table 6.** The top five coefficients of determination ( $r^2$ ) for the relationships between vegetation indices based on the wavebands of FORMOSAT-2 (F2), RapidEye (RY), WorldView-2 (WV2) and plant N uptake (PNU), nitrogen nutrition index (NNI) at the panicle initiation (PI), stem elongation (SE), heading (HE), and across stages (All), respectively. Only significant  $r^2$  values were listed.

PI Stage		SE Stage		HE Stage		All	
Index	PNU	Index	PNU	Index	PNU	Index	PNU
F2-CI	0.39 **	F2-CI	0.52 **	F2-CI	0.50 **	F2-CI	0.81 **
F2-GNDVI	0.35 **	F2-TV1	0.52 **	F2-GNDVI	0.48 **	F2-RVI	0.77 **
F2-TCARI/OSAVI	0.34 **	F2-GNDVI	0.50 **	F2-RVI	0.40 **	F2-MCARI/OSAVI	0.76 **
F2-RVI	0.33 **	F2-OSAVI	0.50 **	F2-NDVI	0.39 **	F2-TCARI/OSAVI	0.76 **
F2-MCARI/OSAVI	0.33 **	F2-MCARI/OSAVI	0.49 **	F2-TCARI/OSAVI	0.36 **	F2-MCARI	0.75 **
RY-MTCI	0.62 **	RY-MTCI	0.64 **	RY-NDPI	0.52 **	RY-NDPI	0.83 **
RY-CCCI	0.59 **	RY-CCCI	0.62 **	RY-RECI	0.52 **	RY-MTCI	0.82 **
RY-NDPI	0.58 **	RY-NDPI	0.61 **	RY-MTCI	0.51 **	RY-CI	0.81 **
RY-RECI	0.46 **	RY-RECI	0.57 **	RY-RETCARI	0.51 **	RY-RECI	0.81 **
RY-NDRE	0.43 **	RY-RETVI	0.56 **	RY-RETCARI/REOSAVI	0.51 **	RY-REMCARI	0.79 **
WV2-NDPI	0.63 **	WV2-NDPI	0.65 **	WV2-RECI	0.62 **	WV2-NDPI	0.82 **
WV2-MTCI	0.60 **	WV2-MTCI	0.64 **	WV2-NDPI	0.61 **	WV2-MTCI	0.82 **
WV2-RETVI	0.54 **	WV2-RETVI	0.61 **	WV2-MTCI	0.61 **	WV2-RECI	0.82 **
WV2-RECI	0.53 **	WV2-RECI	0.60 **	WV2-NDRE	0.61 **	WV2-CI	0.81 **
WV2-NDRE	0.52 **	WV2-NDRE	0.59 **	WV2-REOSAVI	0.61 **	WV2-REMCARI	0.81 **
Index	NNI	Index	NNI	Index	NNI	Index	NNI
F2-CI	0.35 **	F2-TCARI	0.34 **	F2-CI	0.58 **	F2-CI	0.32 **
F2-TCARI/OSAVI	0.32 **	F2-TCARI/OSAVI	0.33 **	F2-GNDVI	0.57 **	F2-TCARI	0.30 **
F2-RVI	0.31 **	F2-MCARI	0.33 **	F2-NDVI	0.48 **	F2-MCARI	0.29 **
F2-GNDVI	0.31 **	F2-MCARI/OSAVI	0.32 **	F2-RVI	0.47 **	F2-TCARI/OSAVI	0.29 **
F2-MCARI/OSAVI	0.29 **	F2-CI	0.30 **	F2-TCARI/OSAVI	0.44 **	F2-RVI	0.28 **
RY-MTCI	0.44 **	RY-REMCARI	0.35 **	RY-NDPI	0.61 **	RY-RETCARI/REOSAVI	0.37 **
RY-NDPI	0.44 **	RY-CCCI	0.34 **	RY-RECI	0.61 **	RY-MTCI	0.37 **
RY-RECI	0.38 **	RY-TCARI	0.34 **	RY-MTCI	0.61 **	RY-NDPI	0.35 **
RY-CCCI	0.36 **	RY-MTCI	0.33 **	RY-NDRE	0.60 **	RY-CCCI	0.35 **
RY-NDRE	0.36 **	RY-REMCARI/REOSAVI	0.33 **	RY-RETCARI/REOSAVI	0.60 **	RY-RETCARI	0.34 **
WV2-MTCI	0.41 **	WV2-NDPI	0.37 **	WV2-RECI	0.62 **	WV2-NDPI	0.37 **
WV2-RECI	0.41 **	WV2-REMCARI	0.36 **	WV2-NDPI	0.61 **	WV2-MTCI	0.35 **
WV2-NDRE	0.41 **	WV2-RETVI	0.36 **	WV2-MTCI	0.61 **	WV2-CCCI	0.35 **
WV2-NDPI	0.40 **	WV2-TCARI	0.34 **	WV2-NDRE	0.61 **	WV2-RECI	0.34 **
WV2-RETVI	0.38 **	WV2-TCARI/OSAVI	0.33 **	WV2-REOSAVI	0.61 **	WV2-REMCARI	0.33 **

\*\* Correlation is significant at the  $p < 0.01$  level; \* Correlation is significant at the  $p < 0.05$  level.

The improvements of RE-based VIs over traditional ones (B, G, R, and NIR bands) were also demonstrated in Figure 3. It is evident that most of the RE-based indices derived from the WorldView-2 bands had the best performance, followed by the RapidEye RE-based indices, and the FORMOSAT-2-based VIs had the worst performance. The slightly better performance of WorldView-2 RE-based indices relative to those of RapidEye might be attributed to the different RE band settings of the two satellite sensors. Particularly, the RE-based Transformed Chlorophyll Absorption Reflectance Index (RETCARI) and RETCARI/RE-based Optimized Soil Adjusted Vegetation Index (REOSAVI) based on RapidEye bands underperformed than the same indices with WorldView-2 bands at the PI stage, but the opposite was true at the HE stage (Figure 3).

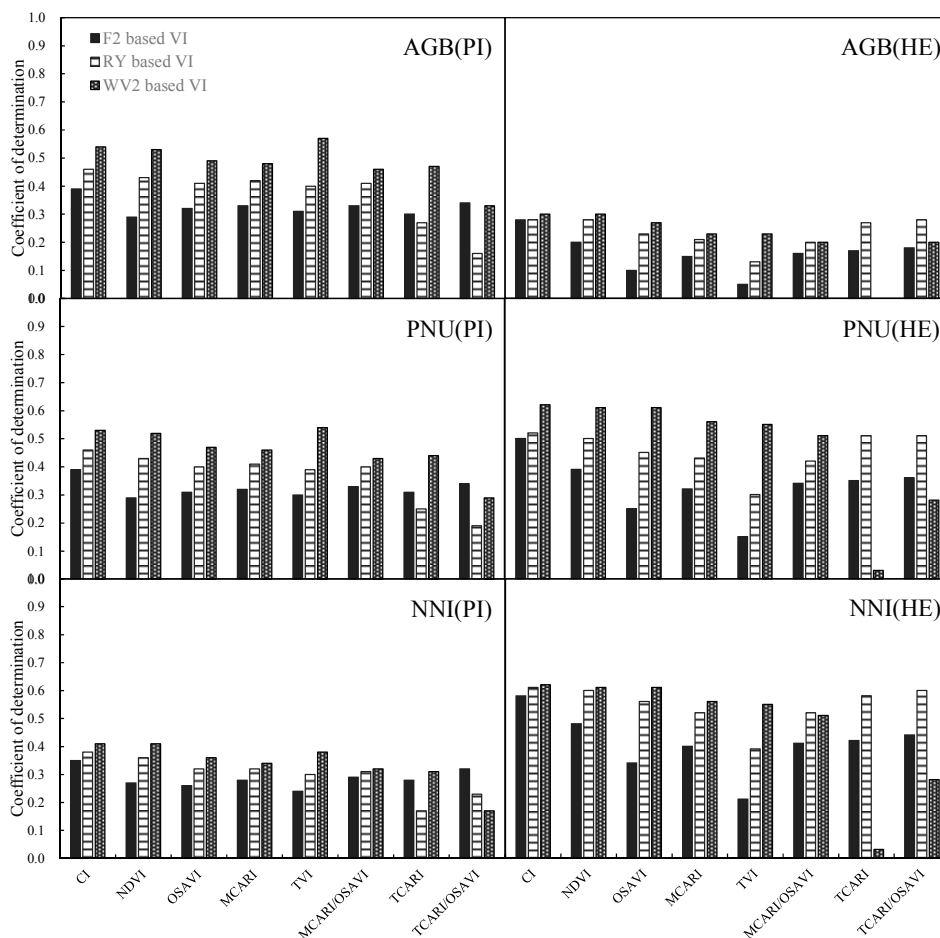


**Figure 3.** Comparison of different vegetation indices (VIs) calculated using FORMOSAT-2 (F2), RapidEye (RY) and WorldView-2 (WV2) satellite data for the relationships with aboveground biomass (AGB), plant N uptake (PNU), and N nutrition index (NNI) at the panicle initiation (PI) and heading (HE) stages, respectively.

### 3.3. Stepwise Multiple Linear Regression Analysis

The SMLR analysis indicated that models using the simulated RapidEye and WorldView-2 bands explained more variability than the ones using FORMOSAT-2 bands at the PI and SE stages (Table 7). The regression results showed that the NIR1 band was the most important band for estimating these N status indicators as it was selected in all the models except the FORMOSAT-2 AGB estimation model at the SE stage. In addition, the RE bands of RapidEye and WorldView-2 were important for AGB, PNU, and NNI estimations at the PI and SE stages (Table 7).

**Table 7.** Stepwise multiple linear regression models based on simulated multi-spectral FORMOSAT-2 (F2), RapidEye (RY), WorldView-2 (WV2) wavebands for estimating aboveground biomass (AGB) and plant N uptake (PNU), nitrogen nutrition index (NNI), and plant N concentration (PNC) at the panicle initiation (PI), stem elongation (SE), heading (HE) and across stages. The wavebands were ranked by the enter order.

	AGB				PNU				NNI				PNC			
	PI	SE	HE	All												
Based on F2 bands																
R <sup>2</sup>	0.61 **	0.51 **	0.29 **	0.82 **	0.60 **	0.66 **	0.50 **	0.81 **	0.45 **	0.30 **	0.57 **	0.36 **	0.08 *	0.22 **	0.51 **	0.43 **
Band	NIR1	R	G	NIR1	NIR1	NIR1	R	NIR1	NIR1	NIR1	R	NIR1	G	R	R	NIR1
	G	B	NIR1	G	G	G	NIR1	G	G		NIR1	G		B	NIR1	R
	B			B	B	B	G	B	B		G	B		NIR1	G	
	R			R	R	R								G		
Based on RY bands																
R <sup>2</sup>	0.68 **	0.55 **	0.29 **	0.82 **	0.66 **	0.68 **	0.50 **	0.82 **	0.46 **	0.50 **	0.59 **	0.38 **	0.07 *	0.20 **	0.57 **	0.43 **
Band	NIR1	NIR1	G	NIR1	NIR1	NIR1	R	NIR1	R	NIR1	R	NIR1	G	R	NIR1	NIR1
	RE	RE	NIR1	RE	RE	RE	NIR1	RE	NIR1	RE	NIR1	RE		B	RE	R
	R	G		R	R	B	RE	R	RE	R	RE	R		NIR1	G	
	B			B	B									G		
Based on WV2 bands																
R <sup>2</sup>	0.76 **	0.63 **	0.31 **	0.82 **	0.71 **	0.69 **	0.52 **	0.82 **	0.52 **	0.49 **	0.61 **	0.38 **	0.09 **	0.10 **	0.56 **	0.43 **
Band	NIR1	NIR1	Y	NIR1	Y	R	R	NIR2								
	RE	RE	NIR1	RE		B	NIR2	R								
	NIR2	G	G	R	R	G			NIR2	R		G			RE	
	C	R			NIR2					Y						
	Y	Y			C											

\*\* Correlation is significant at the  $p < 0.01$  level; \* Correlation is significant at the  $p < 0.05$  level.

At the HE stage, the  $R^2$  values for all the SMLR AGB models were similar (0.29–0.31) based on the three sensor datasets (Table 7). Better  $R^2$  values were achieved for PNU ( $R^2 = 0.50$ – $0.52$ ), PNC ( $R^2 = 0.51$ – $0.57$ ) and NNI ( $R^2 = 0.57$ – $0.61$ ) estimations at this stage than previous ones. The SMLR models outperformed the VI-based models for estimating PNC; however, none of the models performed satisfactorily at the PI and SE stages (Table 7). Compared to the best-performed VI models for estimating all four N indicators, the SMLR models yielded higher  $R^2$  at the PI and SE stages, but similar  $R^2$  at the HE stage and across the stages (Tables 5–7).

In general, AGB and PNU were best estimated at the early growth stage (PI) and across the stages while NNI and PNC were best estimated at the later stage (HE). In most cases, the regression models based on the simulated WorldView-2 bands had the highest performance for AGB, PNU, and NNI estimations at a specific growth stage.

### 3.4. Partial Least Squares Regression Modeling

Table 8 presents the  $R^2$  and RMSEC of Calibration (RMSEC) values of the PLSR models for the four N indicators using the entire spectra of the three simulated satellite bands. According to the  $R^2$  and RMSEC values, the WorldView-2 band-based PLSR models significantly outperformed all the FORMOSAT-2-based ones while the RapidEye-based PLSR models achieved slightly better results than the FORMOSAT-2 ones. However, the performance gaps were much smaller at the HE stage and across the three stages.

**Table 8.** Aboveground biomass (AGB), plant N concentration (PNC), plant N uptake (PNU), and nitrogen nutrition index (NNI) modeling (calibration subset) by partial least square regression (PLSR) analysis using the wavelengths based on the FORMOSAT-2(F2), RapidEye (RY), WorldView-2(WV2) datasets at the panicle initiation (PI), stem elongation (SE), heading (HE) and across stages (All). All  $R^2$  values are significant ( $p < 0.01$ ). RMSEC stands for the RMSE of calibration subset.

	AGB				PNC			
	PI	SE	HE	All	PI	SE	HE	All
Based on F2 bands								
$R^2$	0.64	0.56	0.31	0.82	0.09	0.22	0.54	0.43
RMSEC	0.30	0.58	1.23	1.11	0.16	0.31	0.19	0.36
Based on RY bands								
$R^2$	0.71	0.57	0.30	0.82	0.11	0.23	0.56	0.44
RMSEC	0.26	0.57	1.24	1.11	0.16	0.31	0.18	0.36
Based on WV2 bands								
$R^2$	0.78	0.67	0.38	0.84	0.24	0.31	0.60	0.43
RMSEC	0.23	0.50	1.17	1.02	0.15	0.29	0.17	0.36
	PNU				NNI			
	PI	SE	HE	All	PI	SE	HE	All
Based on F2 bands								
$R^2$	0.62	0.68	0.50	0.81	0.46	0.50	0.58	0.36
RMSEC	7.76	9.61	25.50	18.32	0.08	0.10	0.15	0.15
Based on RY bands								
$R^2$	0.69	0.69	0.50	0.82	0.49	0.52	0.59	0.36
RMSEC	7.02	9.44	25.44	18.05	0.08	0.10	0.15	0.15
Based on WV2 bands								
$R^2$	0.75	0.78	0.55	0.83	0.55	0.56	0.62	0.43
RMSEC	6.24	7.87	24.22	17.56	0.07	0.09	0.15	0.14

Similar to the SMLR analysis, AGB and PNU were best estimated at the PI stage and across the stages by the PLSR method, whereas NNI and PNC were best estimated at the HE stage. The PLSR

and SMLR methods had similar performance for the AGB and PNU estimations while better  $R^2$  and RMSEC values were found in the PLSR models for NNI and PNC estimations in most cases. Especially for the PNC estimation, the PLSR models based on the WorldView-2 bands explained significantly more variability ( $R^2 = 0.24\text{--}0.31$ ) compared to the counterparts of SMLR models ( $R^2 = 0.09\text{--}0.10$ ) at the PI and SE stages.

In addition, the calculated VIP values revealed that for AGB and PNU estimation, the NIR bands, especially the NIR1 centered at 830 nm was the most important one in the PLSR models in most cases (Figures 4 and 5). In contrast, for PNC estimation, the VIP scores indicated that the most important band changed from G band (for FORMOSAT-2 and RapidEye) at the PI stage to R band at the SE stage, and finally to NIR1 band at the HE stage (Figure 6a–c). For NNI estimation, the NIR1 band was consistently important (Figure 6d–f). The R band at the PI stage (Figure 6d), G band at the SE stage (Figure 6e) and both G and R bands at the HE stage were important for NNI estimation. The RE band showed relatively high VIP values at the SE stage for both AGB and PNU estimations and at the PI stage for PNC estimation. The Y band of WorldView-2 demonstrated its importance at the HE stage for AGB, PNU, and NNI estimations. Notably, the Y band had high VIP values for PNC estimation from PI thru HE stages. The C band of WorldView-2 also had VIP values close to or above “1” for AGB and PNU estimations at the SE stage (Figures 4–6).

### 3.5. Validation of the Estimation Models

The validation results of the three types of models were summarized in Table 9. The VI-based PNC model validation for the PI stage was excluded since no significant relationship was identified. For AGB and PNU estimations, the RapidEye and WorldView-2 band-based VI models had significantly higher  $R^2$  than those based on FORMOSAT-2 bands while the validation results of the former two types of models were more comparable at the PI and SE stages (Table 9). The SMLR and PLSR validation models showed similar results. However, the FORMOSAT-2-based SMLR and PLSR models had significantly higher  $R^2$  and lower RMSE and REr compared to the counterparts of VI models. For PNC estimation, the WorldView-2 band-based PLSR models had significantly higher  $R^2$  than those of FORMOSAT-2-based models at the PI and SE stages (Table 9). In most cases, the SMLR and PLSR models showed better performance for estimating the four N indicators than the VI models.

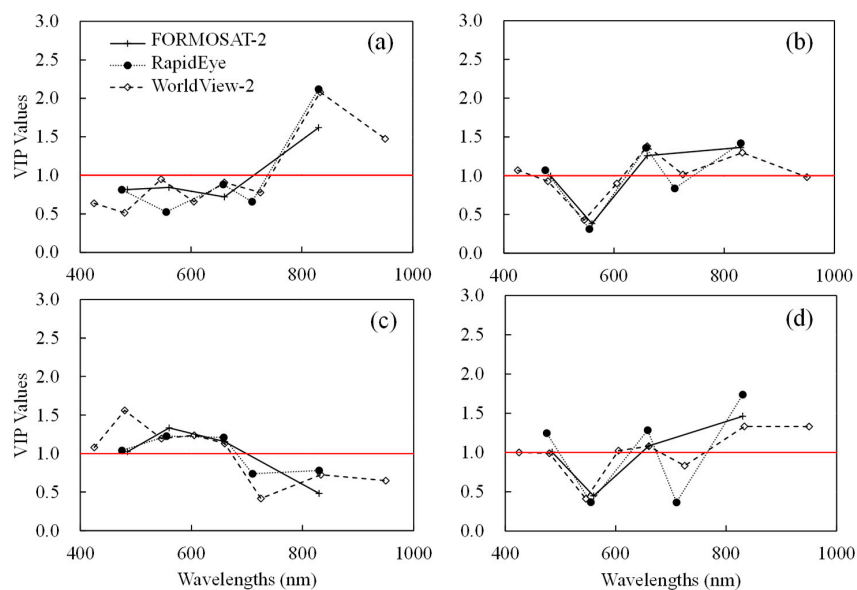


**Figure 4.** Variable Importance in Projection (VIP) values as function of wavelengths formatted to FORMOSAT-2, RapidEye, and WorldView-2 spectra for aboveground biomass (AGB) estimation at: the panicle initiation (PI) (a); stem elongation (SE) (b); heading (HE) (c); and across stages (d).

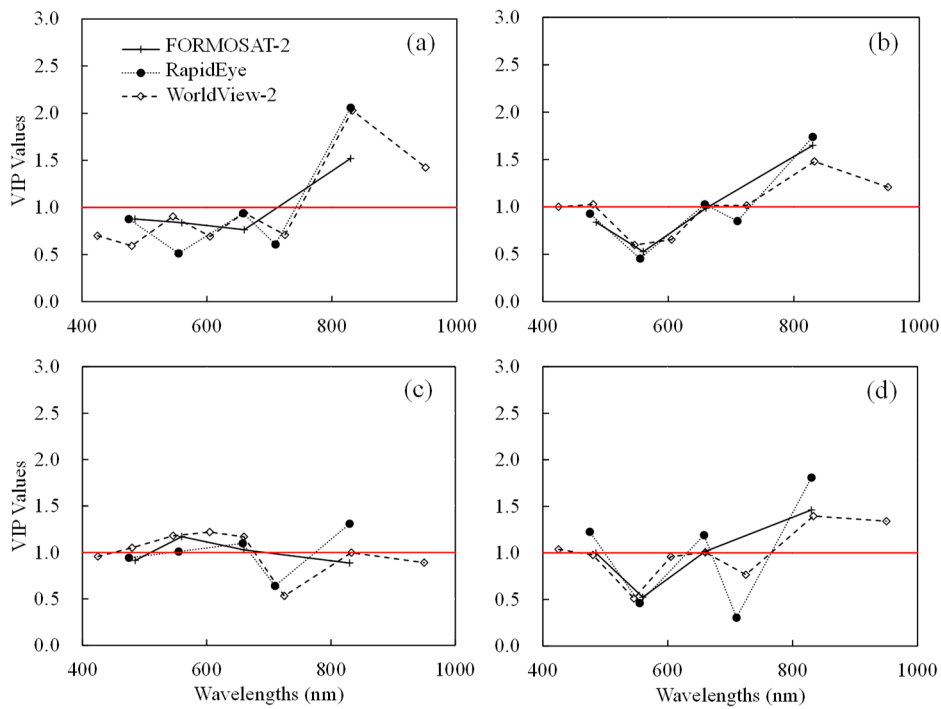


**Figure 5.** Variable Importance in Projection (VIP) values as function of wavelengths formatted to FORMOSAT-2, RapidEye, and WorldView-2 spectra for plant N uptake (PNU) estimation at: the panicle initiation (PI) (a); stem elongation (SE) (b); heading (HE) (c); and across stages (d).

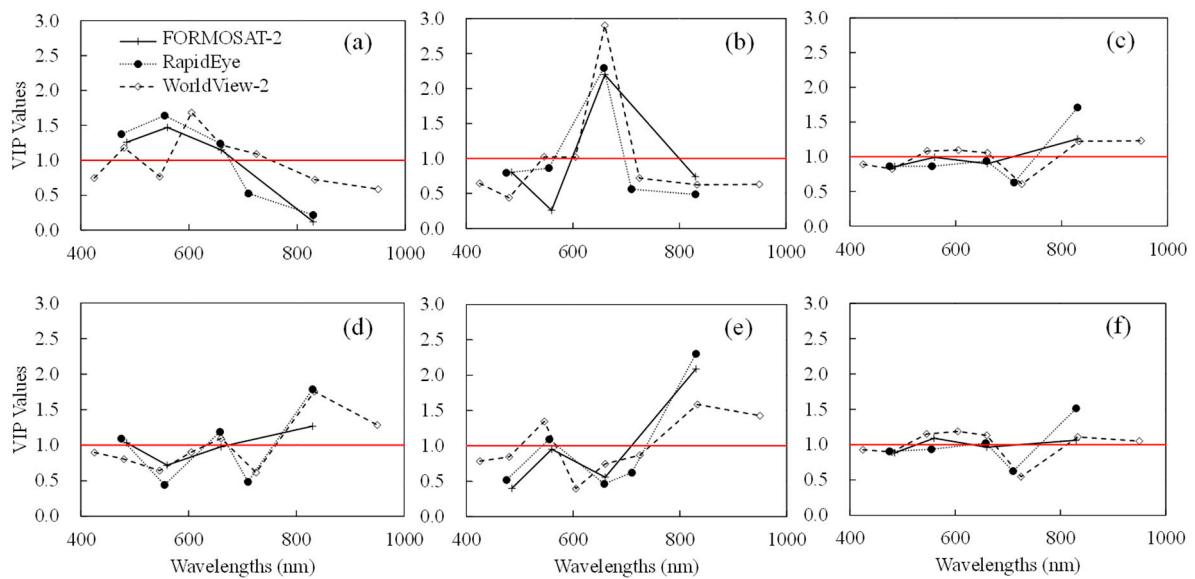


**Figure 6.** Variable Importance in Projection (VIP) values as function of wavelengths formatted to FORMOSAT-2, RapidEye, and WorldView-2 spectra for plant N concentration (PNC) estimation at: the panicle initiation (PI) (a); stem elongation (SE) (b); and heading (HE) (c) stages; and for N nutrition index (NNI) estimation at: the PI (d); SE (e); and HE (f) stages.

**Table 9.** Comparison of the validation results for the best performed vegetation indices (VIs), the stepwise multiple linear regression (SMLR) models, and the partial least squares regression (PLSR) models for biomass (AGB), plant N uptake (PNU), nitrogen nutrition index (NNI), and plant N concentration (PNC) estimations at the panicle initiation (PI), stem elongation (SE) and heading (HE) stages. RMSEP stands for the RMSE of validation subset.

	AGB									PNU								
	PI			SE			HE			PI			SE			HE		
	F2	RY	WV2															
Best performed VI-based models																		
R <sup>2</sup>	0.36	0.76	0.64	0.57	0.73	0.75	0.26	0.28	0.32	0.37	0.73	0.62	0.66	0.78	0.72	0.47	0.46	0.45
RMSEP	0.39	0.24	0.29	0.67	0.53	0.70	1.27	1.25	1.23	9.33	6.16	7.27	10.92	8.71	9.73	23.77	24.06	24.20
REr (%)	36.56	22.73	27.40	36.90	29.08	38.35	21.46	21.13	20.66	35.75	23.61	27.88	26.43	21.08	23.54	24.91	25.22	25.36
SMLR-based models																		
R <sup>2</sup>	0.69	0.77	0.85	0.65	0.77	0.82	0.39	0.39	0.39	0.73	0.78	0.84	0.76	0.78	0.76	0.49	0.50	0.49
RMSEP	0.27	0.23	0.19	0.62	0.53	0.45	1.19	1.19	1.18	6.27	5.56	4.74	9.83	9.28	9.36	23.04	22.98	23.14
REr (%)	25.56	21.95	17.81	33.90	28.87	24.78	19.98	19.99	19.83	24.03	21.30	18.16	23.79	22.45	22.66	24.14	24.08	24.25
PLSR-based models																		
R <sup>2</sup>	0.65	0.77	0.84	0.76	0.79	0.78	0.38	0.39	0.33	0.70	0.77	0.81	0.76	0.77	0.72	0.50	0.49	0.47
RMSEP	0.28	0.23	0.19	0.55	0.52	0.48	1.18	1.18	1.23	6.49	5.59	5.12	9.76	9.34	9.92	23.07	23.14	23.54
REr (%)	26.79	21.62	18.10	30.27	28.45	26.17	19.91	19.93	20.72	24.88	21.43	19.64	23.63	22.59	24.01	24.18	24.26	24.68
NNI																		
PNC																		
	NNI									PNC								
	PI			SE			HE			PI			SE			HE		
	F2	RY	WV2															
Best performed VI-based models																		
R <sup>2</sup>	0.37	0.45	0.41	0.28	0.32	0.27	0.43	0.41	0.38	-	-	-	0.13	0.02	0.24	0.26	0.24	0.20
RMSEP	0.08	0.07	0.08	0.11	0.10	0.11	0.17	0.18	0.18	-	-	-	0.33	0.34	0.31	0.25	0.26	0.27
REr (%)	8.41	7.79	8.14	10.31	10.06	10.94	16.28	16.81	17.29	-	-	-	13.77	14.44	13.1	15.67	16.17	16.67
SMLR-based models																		
R <sup>2</sup>	0.55	0.52	0.44	0.28	0.25	0.30	0.46	0.48	0.46	0.12	0.11	0.09	0.25	0.21	0.37	0.30	0.36	0.30
RMSEP	0.07	0.07	0.07	0.11	0.11	0.11	0.17	0.16	0.17	0.19	0.20	0.20	0.30	0.31	0.29	0.24	0.23	0.24
REr (%)	7.18	7.28	7.86	10.34	11.05	10.44	15.81	15.48	15.89	7.92	7.94	7.97	12.58	12.98	12.36	15.19	14.48	15.17
PLS-based models																		
R <sup>2</sup>	0.62	0.56	0.54	0.28	0.27	0.24	0.48	0.47	0.44	0.14	0.21	0.34	0.25	0.30	0.48	0.36	0.35	0.30
RMSEP	0.06	0.07	0.07	0.11	0.11	0.11	0.16	0.16	0.17	0.19	0.19	0.17	0.30	0.29	0.25	0.23	0.23	0.25
REr (%)	6.68	7.00	7.14	10.53	10.70	10.81	15.44	15.64	16.12	7.85	7.62	6.96	12.64	12.27	10.56	14.43	14.65	15.41

## 4. Discussion

### 4.1. Impacts of Growth Stages on N Status Monitoring

The AGB increased notably while the PNC decreased steadily over the growth stages in this study (Table 4), which conformed to many previous studies [43,44,63,64]. Because PNU is a product of AGB and PNC, plants with high PNC and low AGB at earlier growth stages may have similar PNU as those with low PNC and higher biomass at later growth stages [47]. Thus, the growth stage is an important reference factor, which must be taken into account when using PNU as an indicator for crop N diagnosis.

Our VI models revealed that rice AGB and PNU were best estimated at the early growth stage while the opposite was true for NNI and PNC. Similarly, Yu et al. (2013) [65] found the VIs performed better for estimating rice PNC after the HE stage. Li et al. (2014) [66] also noted that PNC was better estimated at later growth stages for maize. This is because that before the HE stage, the N accumulation rate is lower than that of biomass; therefore, the later dominates canopy reflectance [65,67]. After the HE stage, the increase in AGB gains slower, and plant N starts to dominate canopy reflectance [65]. Huang et al. (2015) [3] proposed an indirect approach to estimate NNI at the PI stage based on the AGB and PNU values derived from FORMOSAT-2 satellite images for guiding topdressing N application at the SE stage. This indirect method might be tested using RE-based VI models derived from RapidEye and WorldView-2 images in the future.

### 4.2. Importance of the Red Edge and Other Bands for N Status Estimation

The use of canopy spectra for N assessment mostly depends on the close relationship between N and chlorophylls in the cell metabolism [68]. The R band-based VIs like NDVI, RVI, and OSAVI are the most common indices in N status estimation. However, the R band can be easily influenced by soil background reflectance at early growth stages when vegetation coverage is small. The NDRE and RECI indices significantly improved the estimation results compared to NDVI and RVI in our research (Tables 5 and 6). This is because the RE reflectance is highly correlated with chlorophyll content [69,70], and is responsive to variation in LAI or biomass [30,71]. In addition, it is insensitive to background effects [72]. Our results also confirmed the findings by Li et al. (2014) [66], who found that the NDRE and RECI improved the PNC and PNU estimations of summer maize. They also proved that the broader bandwidth led to decreased performance of NDVI and RVI while no significant effect was identified for NDRE and RECI.

The RE-based index, MTCI, had the best performance in this study. According to Li et al. (2014) [66], the broad band MTCI performed slightly better than the narrow ones. In our study, the broadband MTCI calculated using the simulated RapidEye and WorldView-2 bands was among the top five indices for AGB, PNU, and NNI estimation models. MTCI was also proven to be highly correlated with the PNC in maize [66] and in rice [65]. It would not saturate at high N treatments [66,68]. Nevertheless, the relationship between MTCI and PNC might be more influenced by soil background at early stages relative to CCCI [66].

The two RE-based indices, CCCI and NDPI, are both two-dimensional indices [59]. The CCCI is calculated based on NDVI and NDRE, while the NDPI is based on NDVI and RECI. Ramoelo et al. (2012) [23] evaluated the CCCI for wheat canopy N content estimation using simulated RapidEye bands, and proved the CCCI performed well for estimating N status indicators. Li et al. (2014) [66] simulated the WorldView-2 wavebands and reported that the CCCI and NDPI improved the estimation results. In our study, the CCCI and NDPI based on RapidEye, and NDPI based on WorldView-2 bands yielded high  $r^2$  for AGB (Table 5), PNU (Table 6), and NNI (Table 6) estimations, similar to previous research. However, the CCCI based on WorldView-2 bands yielded slightly lower  $r^2$  than that of RapidEye at early stages. Different RE band settings might lead to the discrepancies of model results. In particular, the RE band of WorldView-2 ranges from 705 to 745 nm, peaking at 725 nm, while the RE band of RapidEye is set to 690–730 nm, peaking at 710 nm. As the crop

develops, the RE position moves to longer wavelength due to higher crop biomass and plant pigment content. Thus, at early growth stages, the RE-based indices using both satellite bands yielded similar  $r^2$ , while the RE indices of WorldView-2 achieved slightly higher  $r^2$  for AGB and PNU estimations than the ones of RapidEye at the HE stage (Tables 5 and 6).

The G band-based GNDVI and CI performed slightly better than the R band-based NDVI and RVI. These results confirmed previous findings by Carter (1993) [73] and Carter and Knapp (2001) [74], who found that G and RE spectra were sensitive to a wider range of chlorophyll levels than R reflectance. Bausch et al. (2010) [27] also reported that G band-based VIs improved N status evaluation compared with R band-based indices. Yu et al. (2013) [65] found two “hot zones” related to N status: RE bands (700–760 nm) paired with RE to NIR spectral region (700–1100 nm) and G bands (500–590 nm) paired with RE to NIR region (700–1100nm), which confirmed the importance of RE, NIR, and G bands for N status estimation.

The NIR1 waveband explained the most variability compared with other wavebands. This was also observed in wheat LAI estimation using PLSR analysis by Herrmann et al. (2011) [75], who revealed different VIP values of NIR band between wheat and potato. For rice LAI, leaf dry weight, leaf N concentration, and leaf N density estimations, PLSR models demonstrated that the bands >760 nm and at 687 nm were most important [38]. The RE band (707 nm) was only important for leaf N concentration as the third latent variable [38]. In our study, the VIP scores indicated it was important to include the RE band at the PI stage for PNC estimation and at the SE stage for AGB and PNU estimations. The Y band of WorldView-2 demonstrated high importance for PNC estimation from PI thru HE stages. In addition, the Y band was significant for estimating all four N status variables at the HE stage whereas the C band was valuable for AGB and PNU estimations at the SE stage. Such results demonstrated the value of having the additional C and Y bands in WorldView-2 sensor for crop N status monitoring. While WorldView-2 data with extra spectral bands have higher potential for improving N status monitoring, considering the cost factor, RapidEye data might be more practical than WorldView-2 data for large-scale studies.

#### 4.3. Limitations of This Study

Physically based canopy reflectance models were not applied in this study because they are complex to design, parameterize, and implement, especially in wet rice paddies. Furthermore, those models can only be inverted to retrieve canopy parameters that are directly involved in physical processes of radiative transfer, such as photosynthetic pigments, instead of N [35]. The VI, SMLR, and PLSR models generated from this study were not validated using actual satellite images. We were able to obtain several FORMOSAT-2 images during our sampling period, but they cannot be used for validation purpose due to their relatively coarse resolution (8 m) and the relatively small size of our experimental fields in this research. However, in our previous research, we have demonstrated the application of using FORMOSAT-2 satellite imagery for monitoring rice N status in this region [3]. Given the frequent cloudy and rainy days during the growing season in major rice planting regions, it is difficult to obtain satellite images within a narrow time window. We could not find any archived RapidEye and WorldView-2 images that matched our field sampling dates for this remote study site. Some new remote sensing technologies, such as all-weather dual-polarimetric TerraSAR-X satellite data [76] and low-altitude remote sensing based on unmanned aerial vehicles (UAVs) [13], may be incorporated to overcome the limitations.

## 5. Conclusions and Future Outlooks

This study simulated the band settings of FORMOSAT-2, RapidEye, and WorldView-2 satellite images to evaluate the potentials of using satellite remote sensing with RE and additional bands to improve estimation of rice N status. The major findings are summarized as follows:

For VI analysis, the best-performed RE-based VIs explained 53%–64% AGB variability and 62%–65% PNU variability, compared to 30%–40% AGB and 39%–52% PNU variability using the CI at the PI and SE stages.

For the NNI estimation, the NPDI based on WorldView-2 bands and MTCI based on RapidEye bands explained 14%–26% more variability than FORMOSAT-2-based indices.

The SMLR analysis indicated the NIR1 band was most important for estimating all four N status indicators. In addition, the RE band improved AGB, PNU, and NNI estimations at all the three stages, especially at the early PI and SE stages.

The PLSR analysis confirmed the significance of NIR band for PNU estimation at all stages. It also revealed that it was important to include RE band for AGB and PNU estimation at the SE stage and for PNC estimation at the PI stage. Similar to the RE band, the C band of WorldView-2 was also valuable for AGB and PNU estimations at the SE stage. Notably, the Y band of Worldview-2 was found to be significant at the later stage (HE) for estimations of all four N status variables. Especially for PNC estimation, Y band showed consistent importance at all three growth stages.

Both the SMLR and PLSR models, especially those based on the WorldView-2 bands, improved the estimations of all variables in most cases compared to the VI approach.

The PLSR method had slightly better performance than the SMLR approach for NNI and PNC estimations in most cases.

Biomass and PNU were best estimated at the PI and across the stages while NNI and PNC were best assessed at the HE stage.

Overall, the analyses based on the simulated WorldView-2 data showed the best results for estimating rice N status, followed by the ones based on the RapidEye data.

In conclusion, this study demonstrated the values of having the RE as well as the additional visible and NIR bands for rice N status monitoring. The VI and linear regression methods used have been proven suitable. Satellite remote sensing with high spatial and temporal resolution provides a promising technology for large-scale crop N monitoring. In the future, the potential of shortwave infrared (SWIR) bands for N status monitoring can be further investigated using WorldView-3 data with eight SWIR bands. Other methods such as artificial neural networks (ANNs) and support vector machines (SVMs) can be tested in order to reveal possible nonlinear relationships in the data. Moreover, airborne or UAV-based hyperspectral images should be explored in future studies as some most important reflectance features related to N content can only be measured by hyperspectral sensors.

**Acknowledgments:** This research was financially supported by National Basic Research Program (2015CB150405), National Key Research Program (2016YFD0200602), the Innovative Group Grant of Natural Science Foundation of China (31421092), the Sino-Norwegian Cooperative SINOGRain project (CHN-2152, 14-0039), and the GIS and RS Group of the University of Cologne, Germany. We thank the staff of Jiansanjiang Bureau of Agricultural Land Reclamation, Qixing Farm and Jiansanjiang Institute of Agricultural Research for their support. We also would like to thank Kang Yu, Lei Gao, Christoph Hütt for their field work and contributions in spectral data collection.

**Author Contributions:** Yuxin Miao and Georg Bareth conceived and guide the study. Shanyu Huang, Martin L. Gnyp, Yinkun Yao, Qiang Cao and Hongye Wang conducted the field experiments. Shanyu Huang performed the data analysis and wrote the original manuscript. Yuxin Miao and Fei Yuan revised the manuscript. Georg Bareth, Victoria I.S.Lenz-Wiedemann and Martin L. Gnyp reviewed and edited the manuscript. All authors read and approved the final manuscript.

**Conflicts of Interest:** The authors declare no conflict of interest.

## References

1. Yao, Y.; Miao, Y.; Huang, S.; Gao, L.; Ma, X.; Zhao, G.; Jiang, R.; Chen, X.; Zhang, F.; Yu, K.; et al. Active canopy sensor-based precision N management strategy for rice. *Agron. Sustain. Dev.* **2012**, *32*, 925–933. [[CrossRef](#)]
2. Zhao, G.; Miao, Y.; Wang, H.; Su, M.; Fan, M.; Zhang, F.; Jiang, R.; Zhang, Z.; Liu, C.; Liu, P.; et al. A preliminary precision rice management system for increasing both grain yield and nitrogen use efficiency. *Field Crop. Res.* **2013**, *154*, 23–30. [[CrossRef](#)]

3. Huang, S.; Miao, Y.; Zhao, G.; Yuan, F.; Ma, X.; Tan, C.; Yu, W.; Gnyp, M.; Lenz-Wiedemann, V.I.S.; Rascher, U.; et al. Satellite remote sensing-based in-season diagnosis of rice nitrogen status in Northeast China. *Remote Sens.* **2015**, *7*, 10646–10667. [[CrossRef](#)]
4. Yao, Y.; Miao, Y.; Cao, Q.; Wang, H.; Gnyp, M.L.; Bareth, G.; Khosla, R.; Yang, W.; Liu, F.; Liu, C. In-season estimation of rice nitrogen status with an active crop canopy sensor. *IEEE J. Sel. Top. Appl. Earth Obs. Remote Sens.* **2014**, *7*, 4403–4413. [[CrossRef](#)]
5. Li, F.; Miao, Y.; Zhang, F.; Cui, Z.; Li, R.; Chen, X.; Zhang, H.; Schroder, J.; Raun, W.R.; Jia, L. In-season optical sensing improves nitrogen-use efficiency for winter wheat. *Soil Sci. Soc. Am. J.* **2009**, *73*, 1566–1574. [[CrossRef](#)]
6. Cao, Q.; Miao, Y.; Feng, G.; Gao, X.; Li, F.; Liu, B.; Yue, S.; Cheng, S.; Ustin, S.; Khosla, R. Active canopy sensing of winter wheat nitrogen status: An evaluation of two sensor systems. *Comput. Electron. Agric.* **2015**, *112*, 54–67. [[CrossRef](#)]
7. Cao, Q.; Miao, Y.; Shen, J.; Yu, W.; Yuan, F.; Cheng, S.; Huang, S.; Wang, H.; Yang, W.; Liu, F. Improving in-season estimation of rice yield potential and responsiveness to topdressing nitrogen application with Crop Circle active canopy sensor. *Precis. Agric.* **2016**, *17*, 136–154. [[CrossRef](#)]
8. Xia, T.; Miao, Y.; Wu, D.; Shao, H.; Khosla, R.; Mi, G. Active optical sensing of spring maize for in-season diagnosis of nitrogen status based on nitrogen nutrition index. *Remote Sens.* **2016**, *8*, 605. [[CrossRef](#)]
9. Schmidt, J.P.; Dellinger, A.E.; Beegle, D.B. Nitrogen recommendations for corn: An on-the-go sensor compared with current recommendation methods. *Agron. J.* **2009**, *101*, 916–924. [[CrossRef](#)]
10. Diacono, M.; Rubino, P.; Montemurro, F. Precision nitrogen management of wheat: A review. *Agron. Sustain. Dev.* **2013**, *33*, 219–241. [[CrossRef](#)]
11. Holland, K.H.; Schepers, J.S. Use of a virtual-reference concept to interpret active crop canopy sensor data. *Precis. Agric.* **2013**, *14*, 71–85. [[CrossRef](#)]
12. Mulla, D.J. Twenty five years of remote sensing in precision agriculture: Key advances and remaining knowledge gaps. *Biosyst. Eng.* **2013**, *114*, 358–371. [[CrossRef](#)]
13. Mulla, D.J.; Miao, Y. Precision Farming. In *Land Resources Monitoring, Modeling, and Mapping with Remote Sensing*; Thenkabail, P.S., Ed.; CRC Press: Boca Raton, FL, USA, 2016.
14. Zhao, Q.; Lenz-Wiedemann, V.I.S.; Yuan, F.; Jiang, R.; Miao, Y.; Zhang, F.; Bareth, G. Investigating within-field variability of rice from high resolution satellite imagery in Qixing Farm County, Northeast China. *ISPRS Int. J. Geo-Inf.* **2015**, *4*, 236–261. [[CrossRef](#)]
15. Beerli, O.; Phillips, R.; Carson, P.; Leibig, M. Alternate satellite models for estimation of sugar beet residue nitrogen credit. *Agric. Ecosyst. Environ.* **2005**, *107*, 21–35. [[CrossRef](#)]
16. Claverie, M.; Demarez, V.; Duchemin, B.; Hagolle, O.; Ducrot, D.; Marais-Sicre, C.; Dejoux, J.F.; Huc, M.; Keravec, P.; Béziat, P.; et al. Maize and sunflower biomass estimation in southwest France using high spatial and temporal resolution remote sensing data. *Remote Sens. Environ.* **2012**, *124*, 844–857. [[CrossRef](#)]
17. Tang, Y.L.; Huang, J.F.; Wang, R.C.; Wang, F.M. Comparison of yield estimation simulated models of rice by remote sensing. *Trans. Chin. Soc. Agric. Eng.* **2004**, *20*, 166–171.
18. Magney, T.S.; Eitel, J.U.; Vierling, L.A. Mapping wheat nitrogen uptake from RapidEye vegetation indices. *Precis. Agric.* **2016**. [[CrossRef](#)]
19. Eitel, J.U.H.; Long, D.S.; Gessler, P.E.; Smith, A.M.S. Using in-situ measurements to evaluate the new RapidEye™ satellite series for prediction of wheat nitrogen status. *Int. J. Remote Sens.* **2007**, *28*, 4183–4190. [[CrossRef](#)]
20. Eitel, J.U.H.; Vierling, L.A.; Litvak, M.E.; Long, D.S.; Schulth, U.; Ager, A.A.; Krofcheck, D.J.; Stoscheck, L. Broadband, red edge information from satellites improves early stress detection in a New Mexico conifer woodland. *Remote Sens. Environ.* **2011**, *115*, 3640–3646. [[CrossRef](#)]
21. Asam, S.; Fabritius, H.; Klein, D.; Conrad, C.; Dech, S. Derivation of leaf area index for grassland within alpine upland using multi-temporal RapidEye data. *Int. J. Remote Sens.* **2013**, *34*, 8628–8652. [[CrossRef](#)]
22. Kim, H.O.; Yeom, J.M. Multi-temporal spectral analysis of rice fields in South Korea using MODIS and RapidEye satellite imagery. *J. Astron. Space Sci.* **2012**, *29*, 407–411. [[CrossRef](#)]
23. Ramoelo, A.; Skidmore, A.K.; Cho, M.A.; Schlerf, M.; Mathieu, R.; Heitkönig, I.M.A. Regional estimation of savanna grass nitrogen using the red-edge band of the spaceborne RapidEye sensor. *Int. J. Appl. Earth Obs. Geoinf.* **2012**, *19*, 151–162. [[CrossRef](#)]

24. Mutanga, O.; Adam, E.; Cho, M.A. High density biomass estimation for wetland vegetation using WorldView-2 imagery and random forest regression algorithm. *Int. J. Appl. Earth Obs. Geoinf.* **2012**, *18*, 399–406. [[CrossRef](#)]
25. Yang, C.M.; Liu, C.C.; Wang, Y.W. Using FORMOSAT-2 satellite data to estimate leaf area index of rice crop. *J. Photogram. Remote Sens.* **2008**, *13*, 253–260.
26. Bsaibes, A.; Courault, D.; Baret, F.; Weiss, M.; Olioso, A.; Jacob, F.; Hagolle, O.; Marloie, O.; Bertrand, N.; Desfond, V.; et al. Albedo and LAI estimates from FORMOSAT-2 data for crop monitoring. *Remote Sens. Environ.* **2009**, *113*, 716–729. [[CrossRef](#)]
27. Bausch, W.C.; Khosla, R. QuickBird satellite versus ground-based multi-spectral data for estimating nitrogen status of irrigated maize. *Precis. Agric.* **2010**, *11*, 274–290. [[CrossRef](#)]
28. Thenkabail, P.S.; Smith, R.B.; Pauw, E.D. Hyperspectral vegetation indices and their relationships with agricultural crop characteristics. *Remote Sens. Environ.* **2000**, *71*, 158–182. [[CrossRef](#)]
29. Mutanga, O.; Skidmore, A.K. Narrow band vegetation indices overcome the saturation problem in biomass estimation. *Int. J. Remote Sens.* **2004**, *25*, 3999–4014. [[CrossRef](#)]
30. Gnyp, M.L.; Miao, Y.; Yuan, F.; Ustin, S.L.; Yu, K.; Yao, Y.; Huang, S.; Bareth, G. Hyperspectral canopy sensing of paddy rice aboveground biomass at different growth stages. *Field Crop. Res.* **2014**, *155*, 42–55. [[CrossRef](#)]
31. Van Niel, T.G.; McVicar, T.R. Current and potential uses of optical remotesensing in rice-based irrigation systems: A review. *Aust. J. Agric. Res.* **2004**, *55*, 155–185.
32. Nguy-Robertson, A.; Gitelson, A.; Peng, Y.; Viñaet, A.; Arkebauer, T.; Rundquist, D. Green leaf area index estimation in maize and soybean: Combining vegetation indices to achieve maximal sensitivity. *Agron. J.* **2012**, *104*, 1336–1347. [[CrossRef](#)]
33. Cao, Q.; Miao, Y.; Wang, H.; Huang, S.; Chen, S.; Khosla, R.; Jiang, R. Non-destructive estimation of rice plant nitrogen status with Crop Circle multispectral active canopy sensor. *Field Crop. Res.* **2013**, *154*, 133–144. [[CrossRef](#)]
34. Kanke, Y.; Tubaña, B.; Dalen, M.; Harrell, D. Evaluation of red and red-edge reflectance-based vegetation indices for rice biomass and grain yield prediction models in paddy fields. *Precis. Agric.* **2016**, *17*, 507–530. [[CrossRef](#)]
35. Stroppiana, D.; Fava, F.; Boschetti, M.; Brivio, P.A. Estimation of nitrogen content in crops and pastures using hyperspectral vegetation indices. In *Hyperspectral Remote Sensing of Vegetation*; Thenkabail, P.S., Lyon, J.G., Huete, A., Eds.; CRC Press: Boca Raton, FL, USA, 2012; pp. 245–262.
36. Wold, S.; Trygg, J.; Berglund, A.; Antti, H. Some recent developments in PLS modeling. *Chemometr. Intell. Lab.* **2001**, *58*, 131–150. [[CrossRef](#)]
37. Hansen, P.M.; Schjoerring, J.K. Reflectance measurement of canopy biomass and nitrogen status in wheat crops using normalized difference vegetation indices and partial least squares regression. *Remote Sens. Environ.* **2003**, *86*, 542–553. [[CrossRef](#)]
38. Nguyen, H.T.; Lee, B.W. Assessment of rice leaf growth and nitrogen status by hyperspectral canopy reflectance and partial least square regression. *Eur. J. Agron.* **2006**, *24*, 349–356. [[CrossRef](#)]
39. Wang, Y.; Yang, Y. Effects of agriculture reclamation on hydrologic characteristics in the Sanjiang Plain. *China Geogr. Sci.* **2001**, *11*, 163–167. [[CrossRef](#)]
40. Yan, M.; Deng, W.; Chen, P. Climate change in the Sanjiang Plain disturbed by large-scale reclamation. *J. Geogr. Sci.* **2002**, *12*, 405–412.
41. Xing, B.; Dudas, M.J.; Zhang, Z.; Qi, X. Pedogenetic characteristics of albic soils in the three river plain, Heilongjiang Province. *Acta Pedol. Sin.* **1994**, *31*, 95–104.
42. Greenwood, D.J.; Neeteson, J.J.; Draycott, A. Quantitative relationships for the dependence of growth rate of arable crops on their nitrogen content, dry weight and aerial environment. *Plant Soil* **1986**, *91*, 281–301. [[CrossRef](#)]
43. Lemaire, G.; Jeuffroy, M.H.; Gastal, F. Diagnosis tool for plant and crop N status in vegetative stage: Theory and practices for crop N management. *Eur. J. Agron.* **2008**, *28*, 614–624. [[CrossRef](#)]
44. Justes, E.; Mary, B.; Meynard, J.M.; Machet, J.M.; Thelier-Huche, L. Determination of a critical nitrogen dilution curve for winter wheat crops. *Ann. Bot.* **1994**, *74*, 397–407. [[CrossRef](#)]
45. Gastal, F.; Farruggia, A.; Hacquet, J. The nitrogen nutrition index of grass can be evaluated through determination of N concentration of upper leaves. In Proceedings of the 2001 11th Nitrogen Workshop, Reims, France, 9–12 September 2001; pp. 449–450.

46. Farruggia, A.; Gastal, F.; Scholefield, D. Assessment of the nitrogen status of grassland. *Grass Forage Sci.* **2004**, *59*, 113–120. [[CrossRef](#)]
47. Chen, P.; Haboudane, D.; Tremblay, N.; Wang, J.; Vigneault, P.; Li, B. New spectral indicator assessing the efficiency of crop nitrogen treatment in corn and wheat. *Remote Sens. Environ.* **2010**, *114*, 1987–1997. [[CrossRef](#)]
48. Cilia, C.; Panigada, C.; Rossini, M.; Meroni, M.; Busetto, L.; Amaducci, S.; Boschetti, M.; Picchi, V.; Colombo, R. Nitrogen status assessment for variable rate fertilization in maize through hyperspectral imagery. *Remote Sens.* **2014**, *6*, 6549–6565. [[CrossRef](#)]
49. Jordan, C.F. Derivation of leaf-area index from quality of light on the forest floor. *Ecology* **1969**, *50*, 663–666. [[CrossRef](#)]
50. Gitelson, A.A.; Viña, A.; Ciganda, V.; Rundquist, D.C.; Arkebauer, T.J. Remote estimation of canopy chlorophyll content in crops. *Geophys. Res. Lett.* **2005**, *32*, L08403. [[CrossRef](#)]
51. Rouse, J.W.; Has, R.H.; Schell, J.A.; Deering, D.W. Monitoring vegetation systems in the great plains with ERTS. In Proceedings of the Third ERTS Symposium (NASA), Washington, DC, USA, 10–14 December 1973.
52. Gitelson, A.A.; Kaufman, Y.J.; Merzlyak, M.N. Use of a green channel in remote sensing of global vegetation from EOS-MODIS. *Remote Sens. Environ.* **1996**, *58*, 289–298. [[CrossRef](#)]
53. Rondeaux, G.; Steven, M.; Baret, F. Optimization of soil-adjusted vegetation indices. *Remote Sens. Environ.* **1996**, *55*, 95–107. [[CrossRef](#)]
54. Daughtry, C.S.T.; Walthall, C.L.; Kim, M.S.; Colstoun, E.B.; McMurtrey, J.E., III. Estimating crown leaf chlorophyll concentration from leaf and canopy reflectance. *Remote Sens. Environ.* **2000**, *74*, 229–239. [[CrossRef](#)]
55. Broge, N.H.; Leblanc, E. Comparing prediction power and stability of broadband and hyperspectral vegetation indices for estimation of green leaf area index and canopy chlorophyll density. *Remote Sens. Environ.* **2000**, *76*, 156–172. [[CrossRef](#)]
56. Haboudane, D.; Miller, J.R.; Tremblay, N.; Zarco-Tejada, P.J.; Dextraze, L. Integrated narrow-band vegetation indices for prediction of crop chlorophyll content for application to precision agriculture. *Remote Sens. Environ.* **2002**, *81*, 416–426. [[CrossRef](#)]
57. Fitzgerald, G.; Rodriguez, D.; O’Leary, G. Measuring and predicting canopy nitrogen nutrition in wheat using a spectral index-The canopy chlorophyll content index (CCCI). *Field Crop. Res.* **2010**, *116*, 318–324. [[CrossRef](#)]
58. Dash, J.; Curran, P.J. The MERIS terrestrial chlorophyll index. *Int. J. Remote Sens.* **2004**, *31*, 5513–5532. [[CrossRef](#)]
59. Clarke, T.R.; Moran, M.S.; Barnes, E.M.; Pinter, P.J.; Qi, J. Planar domain indices: A method for measuring a quality of a single component in two-component pixels. In Proceedings of the IGARSS 2001: IEEE International Geoscience and Remote Sensing Symposium, Sydney, Australia, 9–13 July 2001.
60. Wu, C.; Niu, Z.; Tang, Q.; Huang, W. Estimating chlorophyll content from hyperspectral vegetation indices: Modeling and validation. *Agric. For. Meteorol.* **2008**, *148*, 1230–1241. [[CrossRef](#)]
61. Chong, I.; Jun, C. Performance of some variable selection methods when multicollinearity is present. *Chemom. Intell. Lab.* **2005**, *78*, 103–112. [[CrossRef](#)]
62. Li, X.; Zhang, Y.; Bao, Y.; Luo, J.; Jin, X.; Xu, X.; Song, X.; Yang, G. Exploring the best hyperspectral features for LAI estimation using partial least squares regression. *Remote Sens.* **2014**, *6*, 6221–6241. [[CrossRef](#)]
63. Plénet, D.; Lemaire, G. Relationships between dynamics of nitrogen uptake and dry matter accumulation in maize crops. Determination of critical N concentration. *Plant Soil* **1999**, *216*, 65–82. [[CrossRef](#)]
64. Ata-Ul-Karim, S.T.; Yao, X.; Liu, X.; Cao, W.; Zhu, Y. Development of critical nitrogen dilution curve of Japonica rice in Yangtze River Reaches. *Field Crop. Res.* **2013**, *149*, 49–158. [[CrossRef](#)]
65. Yu, K.; Li, F.; Gnyp, M.L.; Miao, Y.; Bareth, G.; Chen, X. Remotely detecting canopy nitrogen concentration and uptake of paddy rice in the Northeast China Plain. *ISPRS J. Photogramm. Remote Sens.* **2013**, *78*, 102–115. [[CrossRef](#)]
66. Li, F.; Miao, Y.; Feng, G.; Yuan, F.; Yue, S.; Gao, X.; Liu, Y.; Liu, B.; Ustin, S.L.; Chen, X. Improving estimation of summer maize nitrogen status with red edge-based spectral vegetation indices. *Field Crop. Res.* **2014**, *157*, 111–123. [[CrossRef](#)]
67. Mistele, B.; Schmidhalter, U. Estimating the nitrogen nutrition index using spectral canopy reflectance measurements. *Eur. J. Agron.* **2008**, *29*, 184–190. [[CrossRef](#)]

68. Shiratsuchi, L.; Ferguson, R.; Shanahan, J.; Adamchuk, V.; Rundquist, D.; Marx, D.; Slater, G. Water and nitrogen effects on active canopy sensor vegetation indices. *Agron. J.* **2011**, *103*, 1815–1826. [[CrossRef](#)]
69. Cho, M.A.; Skidmore, A.K. A new technique for extracting the red edge position from hyperspectral data: The linear extrapolation method. *Remote Sens. Environ.* **2006**, *101*, 181–193. [[CrossRef](#)]
70. Clevers, J.G.P.W.; De Jong, S.M.; Epema, G.F.; Van Der Meer, F.D.; Bakker, W.H.; Skidmore, A.K.; Scholte, K.H. Derivation of the red edge index using the MERIS standard band setting. *Int. J. Remote Sens.* **2002**, *23*, 3169–3184. [[CrossRef](#)]
71. Haboudane, D.; Tremblay, N.; Miller, J.R.; Vigneault, P. Remote estimation of crop chlorophyll content using spectral indices derived from hyperspectral data. *IEEE Trans. Geosci. Remote Sens.* **2008**, *46*, 423–437. [[CrossRef](#)]
72. Zarco-Tejada, P.J.; Miller, J.R.; Morales, A.; Berjon, A.; Aguera, J. Hyperspectral indices and model simulation for chlorophyll estimation in open-canopy tree crops. *Remote Sens. Environ.* **2004**, *90*, 463–476. [[CrossRef](#)]
73. Carter, G.A. Responses of leaf spectral reflectance to plant stress. *Am. J. Bot.* **1993**, *80*, 239–243. [[CrossRef](#)]
74. Carter, G.A.; Knapp, A.K. Leaf optical properties in higher plants: Linking spectral characteristics to stress and chlorophyll concentration. *Am. J. Bot.* **2001**, *88*, 677–684. [[CrossRef](#)] [[PubMed](#)]
75. Herrmann, I.; Pimstein, A.; Karnieli, A.; Cohen, Y.; Alchanatis, V.; Bonfil, D.J. LAI assessment of wheat and potato crops by VEN $\mu$ S and Sentinel-2 bands. *Remote Sens. Environ.* **2011**, *115*, 2141–2151. [[CrossRef](#)]
76. Koppe, W.; Gnyp, M.L.; Hütt, C.; Yao, Y.; Miao, Y.; Chen, X.; Bareth, G. Rice monitoring with multi-temporal and dual-polarimetric TerraSAR-X data. *Int. J. Appl. Earth Obs. Geoinf.* **2013**, *21*, 568–576. [[CrossRef](#)]



© 2017 by the authors. Licensee MDPI, Basel, Switzerland. This article is an open access article distributed under the terms and conditions of the Creative Commons Attribution (CC BY) license (<http://creativecommons.org/licenses/by/4.0/>).